Numerical Calculation of Particle-Laden Gas Flows Past Tubes

A numerical study has been conducted for the flow of a dilute particle-laden gas moving past one or more tubes undergoing erosion. A nonorthogonal body-fitted coordinate system was used to calculate three tube configurations for laminar and turbulent flow regimes. The assumption of one-way coupling allows the calculation of individual particle velocities from the fluid flow field. The significant effects of turbulent velocity fluctuations are taken into account by means of the stochastic separated flow model. The particle flow field information is then used to predict circumferential distributions of particle flux and erosion. Predictions of trajectories for the case of two in-line tubes show that particles with inertia numbers $\lambda > 1$ will strike many tubes in a tube bank due to particle rebounding from tube surfaces. By contrast, particles with $\lambda < 1$ are entrained in the bulk flow between tubes. In general, the effect of increasing the particle-gas suspension temperature is to couple the particle-fluid motion more closely through viscous drag and, thus, to decrease erosion.

M. J. Schuh
C. A. Schuler
J. A. C. Humphrey
Department of Mechanical Engineering
University of California
Berkeley, CA 94720

Introduction

The problem of interest

The erosion of tubes in tube banks by particles suspended in gas flows is a major problem in the power industry. Such erosion is especially important in the reheaters and economizers of coal-fired boilers utilizing fluidized bed combustors. A survey of the literature on the subject, available in Schuh (1987), has uncovered a considerable amount of work on single-phase flow and heat transfer for single tubes, but less for the case of tube banks. In addition, much of what is available for tube banks tends to be semiempirical or qualitative in nature and often in the vein of correlations for predicting overall values of pressure drop and heat transfer. The level of corresponding information relating to particle-laden gas flows, especially the effects of fluid motion on particle motion and hence on tube erosion, is virtually nil.

The study reported here is part of a research effort aimed at measuring and rendering predictable the flow of dilute concentrations of solid spherical particles suspended in isothermal gas streams moving past one or two in-line tubes, or past a tube in a tube bank. The turbulent flow regime is of special interest for which, computationally, the condition of statistical stationarity is assumed. The three configurations of interest are shown in Figure 1. Experimental measurements of the circumferential distributions of particle flux for the one and two in-line tubes in the figure have been reported by Schweitzer and Humphrey (1988) who argue that particle flux, as opposed to erosion where material properties intervene, is a more fundamental quantity to determine experimentally for guiding and testing numerical models for predicting particle motion and surface erosion.

Related work

A review of work pertinent to this study, concerning flow past tubes and the numerical modeling of dilute particle-laden gas flows, has been given by Schuh (1987). A summary of his main findings is provided here.

Particle Tracking and Erosion. The prediction of erosion requires that individual particle speeds and trajectories be known. For this, a Lagrangian formulation of the particle equation of motion is necessary. In order to be able to neglect particle-particle interactions in such a formulation, the particle volume fraction of a solid-gas suspension must be less than approximately 0.001 (Pourahmadi and Humphrey, 1983). In such dilute suspensions, provided that the average particle size is

C. A. Schuh is presently with Astron Research and Engineering, 130 Kifer Court, Sunnyvale, CA 94086.
Correspondence concerning this paper should be addressed to J. A. C. Humphrey.

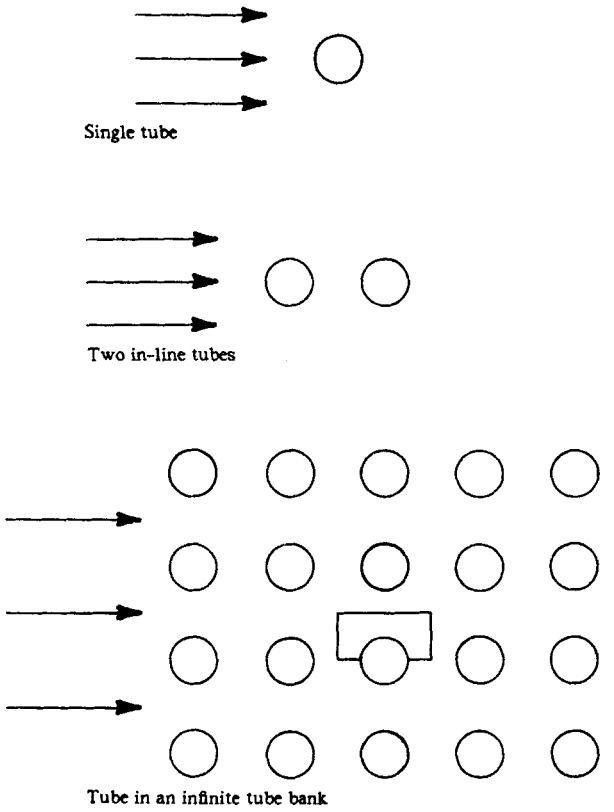

Figure 1. Three flow configurations.

several orders of magnitude smaller than the largest eddies in the flow, one-way (fluid to particle) coupling may be assumed.

Studies using a Lagrangian formulation approach include Laitone (1979a, b, c, 1983; Benchaita et al. 1983; Dosanjh and Humphrey, 1985; Vittal and Tabakoff, 1986; Shuen et al., 1983, 1985; Ormancey and Martinon, 1984). Laitone's work was crucial for demonstrating that fluid mechanic effects alone account for the 2.0–4.6 range in the exponent, m, of the free stream velocity, U, in the expression for erosion, E; $E \propto U^m$. Similarly, the study of Dosanjh and Humphrey established the importance of accounting for the turbulent nature of particle-laden erosive flows. In that study, the authors point to the need for performing erosive wear experiments under carefully controlled fluid mechanic conditions. In contrast to the deterministic approach used by Dosanjh and Humphrey to simulate particle-turbulence interactions, Shuen et al., and Ormancey and Martinon have developed respective approaches that account explicitly for random particle-eddy interactions. The present study builds upon the type of methodology developed by Shuen et al.

Numerical Calculation of Turbulent Flow Past Tubes. While this topic has been the subject of considerable research for the case of a single tube in a free stream, little work exists for the cases of two in-line tubes or a tube in a tube bank. Single tubes have been investigated by, for example, Celik et al. (1985) and Majumdar and Rodi (1985). The latter show that the assumption of a statistically stationary flow leads to inaccurate predictions in the wake region when the approaching flow is irrotational and transition to turbulence must occur in the boundary layer developing along the tube surface. Notwithstanding, highly refined grid predictions of mean flow quantities obtained with a two-equation model of turbulence, using either cylindrical polar coordinates or a streamline/potential grid, are in reasonable agreement with the data available. The laminar flow experiments of Taneda (1956), Grove et al. (1964), Acrivos et al. (1968), and Coutanceau and Bouard (1977), as well as the laminar flow calculations of Majumdar and Rodi, represent important test cases for present validation purposes.

Launder and Massey (1978), Antonopoulos (1979, 1985), Fujii et al. (1984), Chilukuri et al. (1987a, b), and Faghri and Rao (1987) have calculated tube bank flows. Except for Antonopoulos, all of these authors used Cartesian or overlapping Cartesian/cylindrical grids to resolve the flows. By contrast, using a two-equation model of turbulence, Antonopoulos (1979) calculated staggered contravariant velocity components on an orthogonal curvilinear grid. The laminar and turbulent flow calculations in Antonopoulos (1979), the laminar flow calculations in Fujii et al. (1984), the laminar flow measurements in Bergelin et al. (1952), and the turbulent flow measurements in Achenbach (1971) are important test cases for the present work. These are all in-line tube bank configurations.

While Schuh's (1987) review also includes work performed on two in-line tube configurations, all of the studies uncovered were of an experimental nature and none has been of sufficient consequence to this work to be reported here. Two extensive reviews of experimental work on flow and heat transfer for single tubes and tube banks have been written by Zukauskas (1972) and Zukauskas and Ziugzda (1985).

Outline of present approach

Following Thompson et al. (1985), we have chosen in this work to predict the flow past one or more tubes by solving finite difference approximations to the conservation equations on a numerically-generated body-fitted nonorthogonal curvilinear coordinate grid. This avoids the cumbersome use of overlapped orthogonal grids and the attendant interpolation practices required to transfer information between grids, as proposed in some of the references above. By using curvilinear coordinates, the ease of specifying boundary conditions (one of the reasons for employing overlapping grids) is retained. Finally, the use of control functions to specify grid line spacings and shapes allows an arbitrary degree of distributed grid refinement, so that any tube configuration of possible interest can be mapped and computed accurately.

For the turbulent flow calculations at high Reynolds number, a two-equation ($k - \epsilon$) model was used. In this model, a logarithmic wall function for velocity is employed to approximate the wall layer. A generalization of the Boussinesq assumption fixes the dependence of the stress on the rate of strain via an isotropic turbulent viscosity. In contrast to the work of Majumdar and Rodi (1985), here the flow approaching the tube(s) is turbulent. This obviates the need to predict transition to turbulence on the tube surface. Implicit is the assumption of a statistically stationary flow and, while this is incorrect for one or two in-line tubes in a free stream, it is not an unreasonable supposition for the case of a tube in an infinite tube bank. In any event, the assumption is necessary if a practical numerical simulation of the problem is to be achieved.

A Lagrangian-formulated deterministic particle equation of motion is solved via an advanced Runge-Kutta method to pre-

dict particle speeds and trajectories once the fluid flow field is known. The effects of turbulence on particle dispersion are included by superposing a random distribution of turbulent eddies upon the calculated mean flow field, as in Shuen et al. By tracking a statistically significant number of particles, released at different initial locations, overall pictures of particle flow fields, surface fluxes and erosion are obtained. The gas-solid suspensions investigated are assumed to be in thermal equilibrium. Because particle response time to a change in fluid motion depends on viscosity, calculations of the particle flow fields for different values of a prescribed fluid viscosity correspond to fluid flow fields evaluated at *different but uniform* temperatures. Upon striking a tube surface, a particle is forced to rebound according to prescribed restitution relations. Particle fragmentation and/or particle rotation are not considered. The restitution relations employed are the simplest that will provide qualitative pictures of real phenomena.

Fluid-Phase Numerical Procedure

This section summarizes the main features of the numerical procedure developed to calculate the fluid phase flow field. By necessity it is brief. A detailed exposition of this and related material is available in Schuh (1987).

Grid generation

To generate nonorthogonal curvilinear coordinate grids, we have followed closely the work by Thompson et al. (1985, 1986, 1987) and the references therein. Coordinate line generation can be accomplished by a variety of procedures including algebraic, elliptic, graphical and hyperbolic generation methods. The elliptic method was chosen for this work because of its ability to produce grids in a reasonable amount of time with controllable line and point distributions on the geometry of interest. In this method, the following Poisson equations can be solved for the coordinate lines ζ and η in a two-dimensional physical domain

$$\nabla^2\zeta = \frac{g_{22}}{g} P \tag{1}$$

$$\nabla^2\eta = \frac{g_{11}}{g} Q \tag{2}$$

However, it is computationally advantageous to solve for x and y, the cartesian coordinates, for fixed values of ζ and η with the following equation

$$g_{22}(r_{\xi\xi} + Pr_\xi) + g_{11}(r_{\eta\eta} + Qr_\eta) - 2g_{12}r_{\xi\eta} = 0 \tag{3}$$

in the transformed or computational domain. The control functions (source terms P and Q in Eqs. 1–3) are used to control the spacing of the ζ and η coordinate lines, respectively. Two methods were used to control the spacing in this work. The first attracts lines to a point or a line by using equations for P and Q wherein the magnitude of the attraction (or repulsion) and the rate at which it is damped can be separately prescribed. The second method involves derivative line spacing control functions, which are used to maintain the same spacings between coordinate lines in the interior of the calculation domain as the spacings imposed on the boundaries of the domain. Of the two, the derivative line spacing approach was the preferred method in this work. For some of the turbulent flow calculations requiring grid points very near a tube surface, a combination of the two methods was necessary in order to obtain an acceptable distribution of points in front and behind the tube.

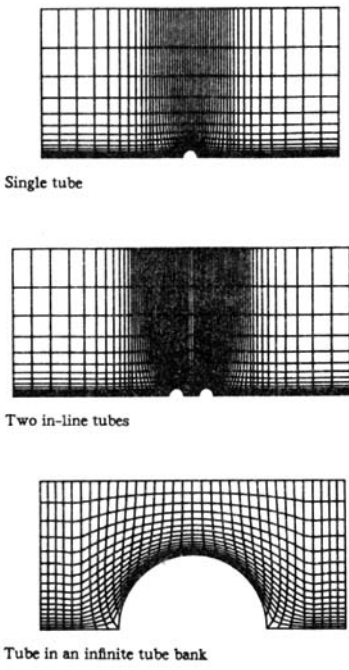

Figure 2. Examples of curvilinear coordinate grids used for the three flow configurations.

Grids are generated in three steps.

- First, a point distribution is chosen on the boundary.
- Then, the interior of the grid is generated by solving Eq. 3.
- Finally, ends are added with the aid of cubic spline interpolation (Press et al., 1986).

The ends are made up of two rectangular cells and an interpolated region between the three points on the end of the interior grid. This procedure is fast and straightforward, while providing orthogonal boundaries which eases the implementation of the outflow and periodic boundary conditions. Figure 2 shows examples of the grids used in this work.

Transport equations and boundary conditions

For steady, two-dimensional, incompressible, constant property, turbulent flow the modeled transport equations written in a conservative form relative to an arbitrary curvilinear coordinate system are:

Continuity of mass

$$(\sqrt{g}\rho U^i)_{\xi^i} = 0 \tag{4}$$

u momentum

$$[\sqrt{g}(\rho U^i u - \mu_e g^{ij} u_{\xi^j})]_{\xi^i} + (y_{\xi^2}P)_{\xi^1} - (y_{\xi^1}P)_{\xi^2} = 0 \tag{5}$$

v momentum

$$[\sqrt{g}(\rho U^i v - \mu_e g^{ij} v_{\xi^j})]_{\xi^i} - (x_{\xi^2}P)_{\xi^1} + (x_{\xi^1}P)_{\xi^2} = 0 \tag{6}$$

Turbulent kinetic energy, k

$$\left[\sqrt{g}\left(\rho U^i k - \frac{\mu_e}{\sigma_k} g^{ij} k_{\xi^j}\right)\right]_{\xi^i} - \sqrt{g}G + \sqrt{g}C_D\rho\epsilon = 0 \qquad (7)$$

Dissipation of turbulent kinetic energy, ϵ

$$\left[\sqrt{g}\left(\rho U^i \epsilon - \frac{\mu_e}{\sigma_\epsilon} g^{ij} \epsilon_{\xi^j}\right)\right]_{\xi^i} - \sqrt{g}C_1 \frac{\epsilon}{k} G + \sqrt{g}C_2\rho \frac{\epsilon^2}{k} = 0 \qquad (8)$$

Generation of turbulent kinetic energy, G

$$G = \mu_t u^i_{x^j}(u^i_{x^j} + u^j_{x^i})$$

$$u^i_{x^1} = \frac{1}{\sqrt{g}}\left[(y_{\xi^2}u^i)_{\xi^1} - (y_{\xi^1}u^i)_{\xi^2}\right]$$

$$u^i_{x^2} = \frac{1}{\sqrt{g}}\left[-(x_{\xi^2}u^i)_{\xi^1} + (x_{\xi^1}u^i)_{\xi^2}\right] \qquad (9)$$

where

$$x^1 = x \quad \text{and} \quad x^2 = y$$

$$\xi^1 = \zeta \quad \text{and} \quad \xi^2 = \eta$$

$$U^i = \boldsymbol{a}^i \cdot (u\hat{\imath} + v\hat{\jmath})$$

$$\boldsymbol{a}^i \equiv \nabla\xi^i$$

$$g^{ij} = \boldsymbol{a}^i \cdot \boldsymbol{a}^j \qquad (10)$$

Here the two-equation ($k - \epsilon$) model of turbulence of Launder and Spalding (1974) has been used; see also Rodi (1982, 1984). In this model:

μ_e is the effective viscosity

$$\mu_e = \mu + \mu_t \qquad (11)$$

μ_t is the turbulent viscosity

$$\mu_t = C_\mu \rho \frac{k^2}{\epsilon} \qquad (12)$$

and the following are empirically determined (or numerically optimized) constants from Rodi (1984):

$$\sigma_k = 1 \quad C_\mu = 0.09 \quad C_1 = 1.44 \quad C_2 = 1.92 \quad C_D = 1$$

$$\sigma_\epsilon = \frac{\kappa^2}{(C_2 - C_1)\sqrt{C_\mu}} \quad \text{and} \quad \kappa = 0.40 \qquad (13)$$

The boundary conditions for the flow fields are shown in Figure 3. For the single tube or the two in-line tubes, u, v, k, and ϵ values are prescribed at the inlet boundary and the flow is assumed to be fully developed at the outlet boundary. The top and bottom boundaries of the solution domain (except for the tube surface) are taken as symmetry planes. On the tube surface, the fluid velocity is zero. For turbulent flow calculations, the equilibrium approximation is used to fix boundary conditions for k and ϵ in the region between the tube surface and the first grid node adjacent to it (Launder and Spalding, 1974).

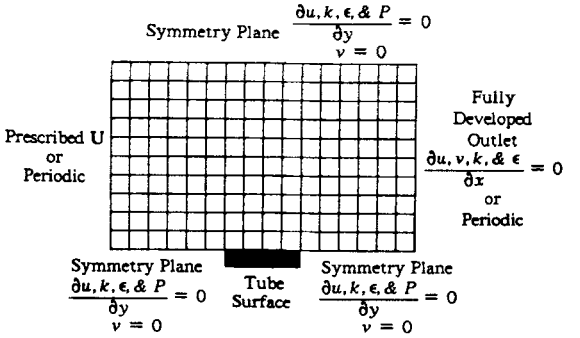

Figure 3. Boundary conditions for the flow field.

In the laminar flow calculations, only the continuity, u momentum, and v momentum equations are solved with the viscosity set to the molecular viscosity, $\mu_e = \mu$. For all cases, the boundary conditions are implemented by using source terms, modification of the convection and diffusion derivatives, or other changes. The velocities, k, and ϵ are prescribed on the inlet plane for the single tube and in-line pair of tubes, so their respective equations are not solved on this plane. However, the pressure is required on the inlet plane (it is used in the pressure derivatives in the momentum equations on the second plane) so the continuity equation is solved to determine the pressure on the inlet plane. (The solution method for the pressure field is discussed in a separate section.) The outlet boundary condition of fully developed flow is implemented by not solving the momentum equations at the exit plane, but by setting the values of the velocities at the exit plane equal to those at the plane directly upstream, and then adjusting these velocities to ensure that continuity of mass is preserved. (In the code, this is implemented by using a grid that is Cartesian for the last three planes and copying the u and v velocities from the plane before the outlet to the outlet plane.) The conservation of mass at the exit plane is assured by correcting the u velocity profile on this plane. For fully developed turbulent flow, the k and ϵ values are also copied from the plane directly upstream of the exit to the exit plane without modification. Like the first plane, the pressure is required on the exit plane so the continuity equation is also solved on the exit plane. The v velocity on the top and bottom symmetry planes and on the tube surface is zero. Therefore the v-momentum equation is not solved on the top and bottom planes. The p, u, k, and ϵ equations are solved on the top and bottom symmetry planes. A very detailed description concerning the practical implementation of these boundary conditions in finite difference form is available in Schuh (1987).

Finite difference approximation

The u, v, k, and ϵ equations can be written in identical form according to

$$[\sqrt{g}(\rho U^i \phi - \Gamma g^{ij}\phi_{\xi^j})]_{\xi^i} - b = 0 \qquad (14)$$

where ϕ is an arbitrary variable, thus admitting a common solution procedure. The equivalent finite difference form of this general equation is readily obtained by a cell or volume integration following the rules and guidelines in Patankar (1980). The

result is

$$A_P\phi_P = A_N\phi_N + A_S\phi_S + A_E\phi_E + A_W\phi_W + S_u \quad (15)$$

where subscripts N, S, E, and W denote the grid points adjacent to P. The upwind-central differencing scheme discussed by Patankar (1980) was used to derive the convection-diffusion A terms in Eq. 15 for the nonstaggered grid used in this work. (The grid used here will be detailed further later.) Detailed expressions for these terms and for linearized forms of the source terms, S_u, are given in Schuh (1987).

The application of Eq. 15 to each variable at each point on the calculation grid yields a set of equations that are solved iteratively. This is accomplished by repeated applications of the tridiagonal matrix algorithm in its standard form (Patankar, 1980) for single and two in-line tubes, and in its cyclic form (Patankar et al., 1977) for the case of a tube in an infinite tube bank.

Treatment of pressure

The calculation of pressure proceeds along the lines of the SIMPLE algorithm of Patankar (1980) by making pressure corrections from iteration to iteration, until the velocities calculated in conjunction with the corrected pressure field satisfy the momentum and continuity equations simultaneously. There are, however, two important differences:

1) A central difference scheme is used for the pressure derivatives in the momentum equations in both the present work and in Patankar's work. This scheme has a $2\Delta\xi^i$ dependence on the type of nonstaggered grid used here, while it has a $\Delta\xi^i$ dependence on a staggered grid. A $2\Delta\xi^i$ dependence results in a pressure oscillation when velocities are averaged to obtain the flux into the control volume used in the pressure calculation. (It is exactly this problem that the staggered grid was created to solve. The staggered grid does not require averages of the velocities to obtain the fluxes into the control volume used in the pressure calculation.) To obviate velocity averaging at the control volume walls, a localized solution of the momentum equation is calculated at each control volume wall. The localized solution of the momentum equation has a $\Delta\xi^i$ dependence in the direction of the two nodes normal to the control volume wall (this is the wall that the flow passes into or out of the control volume) and a $2\Delta\xi^i$ dependence in the tangential direction. The use of the localized solution of the momentum equation eliminates any pressure oscillations in the solution.

2) Pressure corrections of the velocities, as performed by Patankar (1980), are dispensed with, since they do not improve the convergence rate enough to offset the added cost of computing them.

Solution algorithm

The overall solution algorithm is iterative in nature and performs the following steps:

1) Guess an initial velocity and pressure flow field. For this, use a flow field from a previous solution or set all the variables equal to the inlet values except for the tube surface where u and v are set to zero.

2) Calculate a new u velocity field.

3) Calculate a new v velocity field using the same A_N, A_S, A_E, A_W, S_P, and C_P values from the u velocity iteration. (The use of the same coefficients is allowed by virtue of the uniform nature of the grid in the transformed $\zeta - \eta$ plane.)

4) Calculate the pressure correction and obtain the new pressure field.

5) If the flow is turbulent, calculate new k and ϵ fields and update the viscosity field.

6) If the calculation has not converged, go to step 2.

Convergence is checked by monitoring the sum of the residuals for each variable over the entire calculation grid. The numerical solution is taken as converged when the largest of the residual error sums is less than 5.0×10^{-4}.

Miscellaneous matters

Location of Variables. The use of a curvilinear grid requires that all the dependent variables be calculated and stored at the intersection of grid lines (the nodes) rather than at staggered (between nodes) grid locations as in Patankar (1980). (This requires the special treatment of pressure described earlier.)

Underrelaxation. All variables are underrelaxed by factors ranging between 0.3 and 0.8 to stabilize and accelerate the calculations.

Localized Solution of the Momentum Equations. The localized solution of the momentum equations is calculated for u and v at two locations relative to each grid point. The location between neighboring points on the ξ^i grid lines is referred to as the u location and the location between neighboring points on

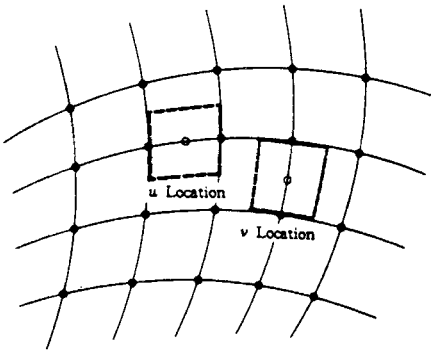

Control volumes for linearized momentum equations

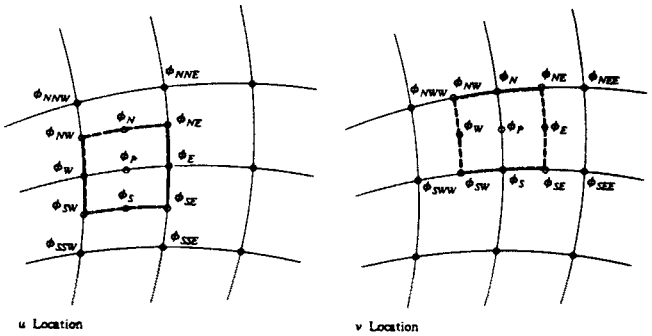

Location of ϕ values on the u location control volume. Location of ϕ values on the v location control volume.

Figure 4. Control volumes used for the localized solution of the momentum equations.

the ξ^2 grid lines is referred to as the v location. These are shown in Figure 4 along with their respective control volumes. This nomenclature of u and v locations is similar to that used in staggered grid configurations. The u and v velocities are calculated at both of these locations by the substitution in Eq. 15 of coefficients derived from flow quantities at the neighboring grid points only. The grid points are indicated for the two control volumes shown in Figures 4b and 4c. The calculated u and v velocities at these locations are referred to as *localized* because they are calculated by using the flow field values from the neighboring points only while the u and v velocities at the intersection of the grid lines are calculated by using an equation solver that includes the global effect of the flow field. Further details are available in Schuh (1987).

Pressure at the Tube Surface. The pressure calculation procedure used in this work results in a slight skewness in the isobars at the tube surface. This is not a serious limitation because as the grid is refined the skewness decreases.

Algorithm Performance. All of the calculations were run on a Digital Equipment Corporation Micro VAX II with 6 Megabytes of memory and a floating point accelerator running Ultrix version 2. The memory requirements for a 119 × 50 grid are 109,568 bytes for the text segment, 18,432 bytes for the initialized data, and 2,885,528 bytes for the uninitialized data. This gives a total memory requirement of 2.87 Megabytes or 506 bytes per grid node. The code uses double precision with 8 bytes per storage location on the Micro VAX II which results in 63 storage locations per grid point. Typical values of convergence time and number of iterations for laminar and turbulent flow are given in Table 1.

Grid Limitations. The grid generation procedure used in this work has difficulty generating grids that change smoothly on the symmetry plane ahead of and behind a tube in the tube bank with spacings less than 1.5 tube diameters. The problem is only serious in a small region for the turbulent flow regime, where jagged mean flow streamlines can result.

Table 1. Characteristics of Algorithm Performance on a Micro Vax II for Maximum Residual Error of 5.0×10^{-4}

Case	CPU Hours	Numerical Iterations	Grid
Laminar Flow*			
Single Tube (Re = 40)	17.8	1,080	119 × 38
Laminar Flow**			
Tube Bank (L/D) = 2, Re = 100)	34.4	3,699	61 × 40
Turbulent Flow†			
Single Tube ($Re = 2.94 \times 10^4$)	28.7	2,026	91 × 28
Turbulent Flow‡			
Tube Bank (L/D) = 2, $Re = 2.56 \times 10^4$)	12.2	1,511	55 × 25

*Calculation initialized by setting the velocity at all grid points to the inlet value and pressure to zero.

**Calculation initialized by setting the velocity at all grid points to one half the average velocity at the minimum cross section and pressure to zero.

†Calculation initialized by setting all variables at all nodes to the inlet values except pressure which was set to zero.

‡As in ** above, but with good estimates of the values for k and ϵ.

Particle-Phase Numerical Procedure

Equation of motion

The following equations are used to describe the motion of an arbitrarily accelerated particle in the fluid flow field

$$\frac{dr_{pt}}{dt} = U_{pt} \tag{16}$$

$$m_{pt}\frac{dU_{pt}}{dt} = m_{pt}g + C_{Dr}\,\tfrac{1}{2}\,\rho|U - U_{pt}|(U - U_{pt})A_{pt} \tag{17}$$

The second equation is the result of a force balance in which, due to the large value of the ratio ρ_{pt}/ρ (2.25×10^3 for glass particles in air), acceleration-dependent drag terms (the added mass and Basset history integral terms) and the lift forces (such as the Magnus and Saffman forces) are negligible. Also small are the pressure gradient forces omitted in the equation. Thus, gravity and drag are the only forces determining the motion of the particle. Equation (17) is taken from Clift et al. [1978], where it is shown that the terms neglected are indeed small compared to those retained. Furthermore, Equation (17) is only valid for non-interacting particles.

It is assumed that the particles are spherical for which, in the creeping flow regime, Stoke's formula for the drag coefficient may be used:

$$C_{Dr} = \frac{24}{Re_{pt}} \tag{18}$$

Since this formula is only valid when the particle Reynolds number, Re_{pt}, is much less than unity, an empirically determined correction factor f is employed when $Re_{pt} \geq 0(1)$. In this work, the following correction factor f given by Boothroyd (1971) was used

$$f = \begin{cases} 1 + 0.15\,Re_{pt}^{0.687} & 0 < Re_{pt} \leq 200 \\ 0.914\,Re_{pt}^{0.282} + 0.0135\,Re_{pt} & 200 < Re_{pt} \leq 2{,}500 \\ 0.0167\,Re_{pt} & 2{,}500 < Re_{pt} \end{cases} \tag{19}$$

Introducing m_{pt} and A_{pt} as defined in the Notation, Eq. 17 is rewritten as

$$\frac{dU_{pt}}{dt} = g + \frac{f}{\tau}(U - U_{pt}) \tag{20}$$

where τ is the particle response time. It is convenient to define a non-dimensional particle response time, or momentum equilibration constant λ, according to:

$$\lambda = \frac{\tau U_{ref}}{L_{ref}} \tag{21}$$

where L_{ref} and U_{ref} are a characteristic length and velocity of the flow field respectively. The quantity λ is the ratio between a time-scale characteristic of the mean particle motion and a time-scale characteristic of the mean fluid flow.

Solution algorithm and boundary conditions

The fourth-order adaptive step size Runge-Kutta scheme in Press et al. (1986) was used to solve Eqs. 16 and 17 subject to the specifications of initial particle location and velocity.

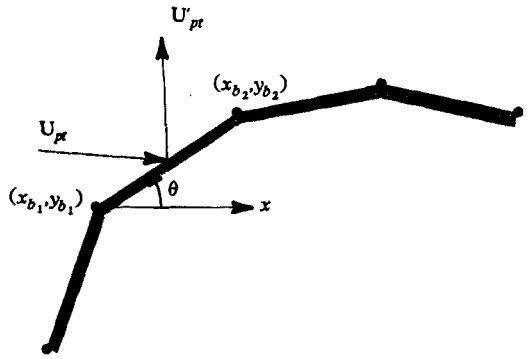

Figure 5. A particle impacting and rebounding from the tube as defined by a series of straight lines.

Special care is required when the particle approaches the tube surface or any other boundary. Figure 5 shows a sketch of a particle impacting and rebounding from the surface of a tube which is defined by a series of straight lines on the curvilinear grid. Because the solution scheme is parabolic in time, a trial and error scheme was implemented to determine the instant and position of impact. For this, a small region around the tube of thickness δ_b is defined. When the particle first approaches the surface, the solution algorithm is unaware of its presence and forces the particle to cross the surface. When this happens, the particle is returned to its previous position, the step size is decreased by a factor of 2, and computation is retried. This procedure is repeated until the particle falls into the δ_b region previously defined. Assuming that the particle velocity remains constant within δ_b, Euler's method is used to determine the position and time of particle impaction (this reduces to finding the intersection of two straight lines). Finally, the velocity of the rebounding particle is calculated assuming constant restitution coefficients for the normal and tangential components of the velocity. Referring to Figure 5, the rebound velocity, U'_{pt}, is calculated by first determining the normal (w_n) and tangential (w_t) velocity components at the boundary from the following equations

$$w_t = u_{pt} \cos\theta + v_{pt} \sin\theta$$
$$w_n = -u_{pt} \sin\theta + v_{pt} \cos\theta \qquad (22)$$

The rebound velocity components normal and tangential to the wall are then calculated using the appropriate restitution coefficients e_t and e_n according to

$$w'_t = e_t w_t$$
$$w'_n = e_n w_n \qquad (23)$$

Finally, the rebound velocity components in the original coordinate system are computed according to

$$u'_{pt} = w'_t \cos\theta - w'_n \sin\theta$$
$$v'_{pt} = w'_t \sin\theta - w'_n \cos\theta \qquad (24)$$

Both restitution coefficients are set to unity at symmetry planes, thus simulating a new particle entering the calculation domain from the opposite direction.

When the particle is very small ($\lambda < 1$), it may rebound from the wall several times. In this case, δ_b must be very small and a very small calculation time step must be used. In this work, δ_b was set to $0.005D$.

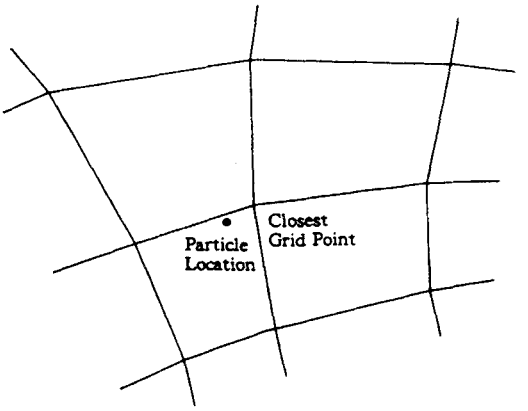

Figure 6a. Particle location and the nearest grid point on a curvilinear grid.

Interpolation of properties on a curvilinear grid

The fluid velocity along the trajectory of a particle must be found by interpolation. Special care is required since the grid used for calculating the velocity field is nonorthogonal. In the present study, an algorithm embodying the following steps was used:

1) Find the grid point closest to the current particle location. (This is called the search step.)

2) Find the cell in which the particle is located, Figure 6a.

3) Divide the cell found in step 2 into four triangles by defining point $c(x_c, y_c)$ in Figure 6b as

$$x_c = \tfrac{1}{4}(x_q + x_r + x_s + x_t) \quad \text{and} \quad y_c = \tfrac{1}{4}(y_q + y_r + y_s + y_t)$$

and then find the triangle in which the particle is located. (Triangle $a - b - c - a$ in Figure 6b.)

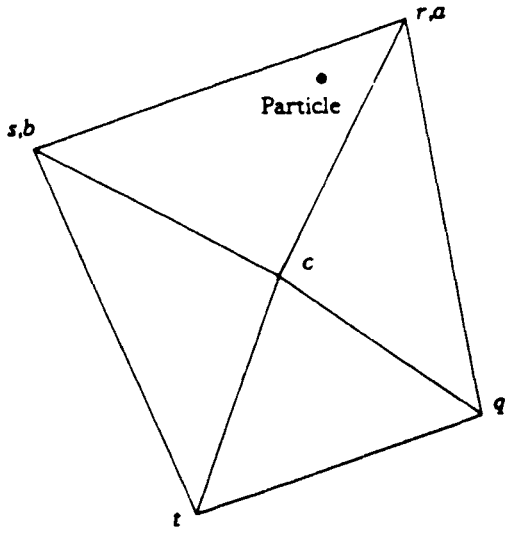

Figure 6b. Division of the grid cell containing the particle into four triangles and the center point $c(x_c, y_c)$.

4) Assume that properties at the center of the grid (point c in Figure 6b) are the mean of the values at the corners of the cell. Linearly interpolate for properties at the particle location using the values at the corners of the triangle $a - b - c - a$ as shown in Figure 6b.)

This procedure ensures continuity of the interpolated properties from cell to cell. It has also proven to be fast to execute numerically. The details of this searching algorithm are given in Schuh (1987).

Influence of turbulent fluctuations

The effect of turbulence on particle dispersion may be neglected when the characteristic particle response time is large compared to the characteristic time of the turbulent fluctuations, i.e., when

$$\tau \gg t_{EDDY} \tag{25}$$

If we assume that the time scale of the turbulent fluctuations is commensurate with the time scale of the mean flow, that is,

$$\frac{L_\epsilon}{u'} \approx \frac{L_{ref}}{U_{ref}} \tag{26}$$

we find that Eq. 25 is equivalent to

$$\lambda \gg 1 \tag{27}$$

In order to account for the effects of relative slip velocity fluctuations and turbulent dispersion when the particle response time is comparable to the time scale of the turbulent fluctuations, i.e., when $\lambda \approx 1$, a stochastic separated flow model (SSF) was used. This model requires an estimate of the mean turbulent characteristics of the flow, which can be obtained anywhere in the flow from the field calculations by extending the interpolation procedure described above to include the kinetic energy, k, and its rate of dissipation, ϵ. Particle trajectories are then computed by solving the instantaneous momentum equations (Eqs. 16 and 17), and superposing random velocity fluctuations on the mean flow field to simulate instantaneous properties of the continuous phase.

The influence of turbulent fluid phase fluctuations on particle trajectories is accounted for through random particle-eddy encounters. However, it should be emphasized that the actual particle motion within an eddy is modeled *deterministically*, as described by the instantaneous momentum equation for the particle. For this, the velocity fluctuations are taken as constant during a particle-eddy interaction.

The key element of the SSF model is to specify eddy properties and particle-eddy interaction times in terms of the mean flow field characteristics. The present approach is along the lines of the work by Shuen et al. (1983). The characteristic velocity fluctuations and lifetime associated with each eddy are found at the start of the particle-eddy interaction. The former are obtained by making a random selection from a probability density function for velocity. For simplicity, the velocity fluctuations are assumed to be isotropic, with a Gaussian PDF having a standard deviation equal to $\sqrt{(2/3)k}$. However, at any instant the x and y velocity components are not necessarily equal.

A particle is assumed to interact with an eddy for a time which is the minimum of either the eddy lifetime or the time required for the particle to cross the eddy. These times are estimated by assuming that the characteristic size of an eddy size is equal to the dissipation length scale,

$$L_\epsilon = \frac{C_\mu^{3/4} k^{3/2}}{\epsilon} \tag{28}$$

with a lifetime given by

$$t_{EDDY} = \frac{L_\epsilon}{u'} = \frac{L_\epsilon}{\sqrt{\frac{2}{3}k}} \tag{29}$$

Due to the stochastic nature of the procedure, many particles have to be simulated in order to obtain an acceptable representation of the average particle flux distribution over the tubes. In the present work, 40 particle trajectories were calculated per each of 100 starting locations uniformly distributed over the inlet plane of the calculation domain, for a total of 4,000 particle trajectories.

Results and Discussion

Test cases

Excellent agreement was found between measurements and calculations of the fluid phase for all the laminar flow cases investigated. For a single tube, these include comparisons of: the width and length of the recirculation zone behind a tube as visualized by Taneda (1956) for $Re = 26$ and 40, and computed by Majumdar and Rodi (1985) for $Re = 40$; the centerline velocity downstream of the tube as measured by Coutanceau and Bouard (1977) for $Re = 40$; the pressure distribution on the tube wall as measured by Grove et al. (1964) for $Re = 40$; the shear stress on the tube wall as measured by Acrivos et al. (1968) for $64 \leq Re \leq 150$. For a tube in a tube bank these include comparisons of the flow streamlines for $Re = 10$ and 100 [$(L/D) = 2.0$]; the flow streamlines and pressure profiles for

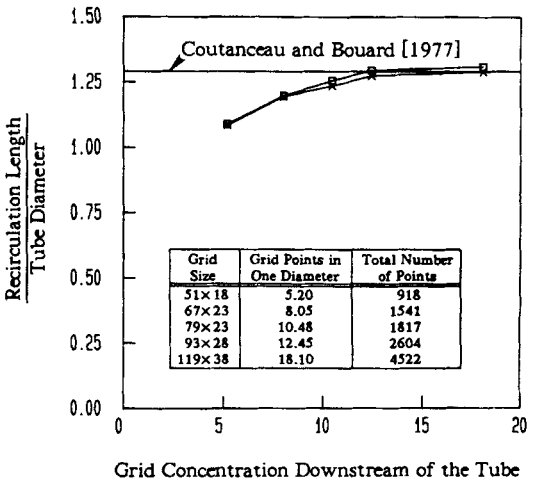

Figure 7. Effect of grid refinement on the recirculation length for $Re = 26$.

Grids used are generated with derivative line spacing with curvature terms only (□) and derivative line spacing with both curvature and spacing terms (×).

Re = 120 [(L/D) = 1.5]; the coefficient of drag as a function of Re for different L/D.

These comparisons, discussed in detail by Schuh (1987), were important for establishing the effects of grid refinement on numerical accuracy for flows free of turbulence model uncertainties. Figure 7 is an example of the type of exercises conducted for single tubes and a tube in a tube bank to generate grid-independent numerical results.

For turbulent fluid motion, comparisons were made with: the channel flow velocity measurements of Laufer (1950) at Re = 61,600; the tube bank calculations of streamlines and turbulent kinetic energy of Antonopoulos (1979) for $Re = 10^6$ [(L/D) = 2] and $Re = 10^5$ [(L_t/D) = 2.06 and (L_l/D) = 1.38]; the surface pressure and shear stress distributions measured for a tube in a tube bank by Achenbach (1971) for $Re = 4 \times 10^5$ (L_t/D) = 2.0 and (L_l/D) = 1.4]; the coefficient of drag as a function of Re for a tube bank with (L/D) = 2.0 as correlated by Zukauskas (1972) and computed by Antonopoulos (1979). For the reasons stated in the Introduction, no attempts were made to predict flows involving transition to turbulence on the tube surface.

The agreement with Laufer's data and that of Antonopoulos at $Re = 10^6$ was quite good. Discrepancies between present calculations and Antonopoulos' results at $Re = 10^5$ were traced to the effects of grid nonorthogonality on numerical diffusion. Thus, we found that by neglecting terms in the turbulence model that account for grid skewness, better agreement could be obtained with Antonopoulos' results. We note that Antonopoulos' method requires an orthogonal grid and provides no means for accounting for nonorthogonality if and when this arises in the *practical implementation* of the code.

The comparisons conducted with respect to Achenbach's pressure data are shown in Figures 8a and 8b. We consider these results to be good indicators of the ability of the code to resolve turbulent flows in tube banks. Grids more refined than 75 × 28 did not yield results better than those shown. The largest discrepancies between measurements and calculations of pressure arise toward the front and rear of the tube, where the assumed law-of-the-wall relation least applies. (This was expected and is a well known failing of the present turbulence model. Notwithstanding, all the qualitative features of the experimental curves are well-represented by the numerical results.) The lack of agreement in pressure suggests that the predicted velocity fields in these regions will also be in error but by a smaller amount proportional to the square root of pressure. This will result in overpredicted velocity magnitudes in the stagnation region and underpredicted values in the wake, which will modify particle trajectories in these regions accordingly.

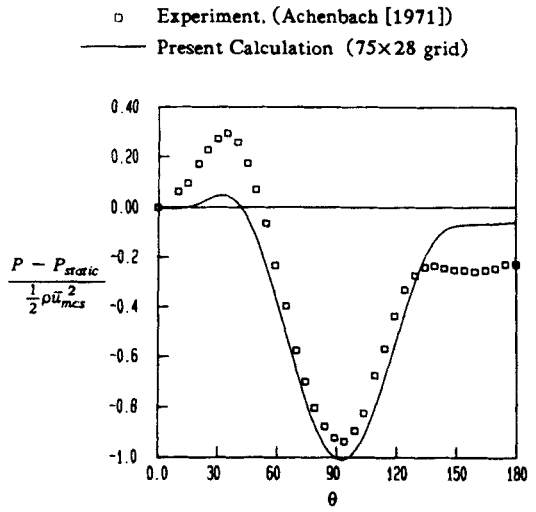

Figure 8a. Pressure distribution on a tube surface for $Re = 4 \times 10^5$, (L_t/D) = 2.0, and (L_l/D) = 1.4 calculation.

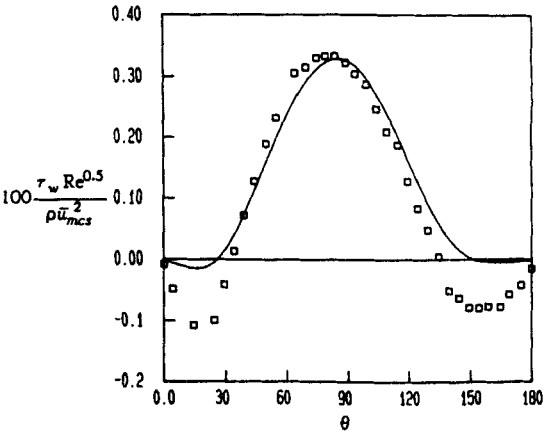

Figure 8b. Shear stress distribution of a tube surface for $Re = 4 \times 10^5$, (L_t/D) = 2.0, and (L_l/D) = 1.4 calculation.

The particle tracking capabilities of the numerical procedure were checked against the analytical results provided by Laitone (1983) for the case of stagnation point flow. Figure 9 shows the very good agreement obtained for three different values of λ. For λ ≤ 0.25 a particle never reaches the surface. For the case λ = 0.5 we have allowed the particle to rebound with values of e_t = 1.0 and e_n = 1.0 set for the restitution coefficients in Eq. 23.

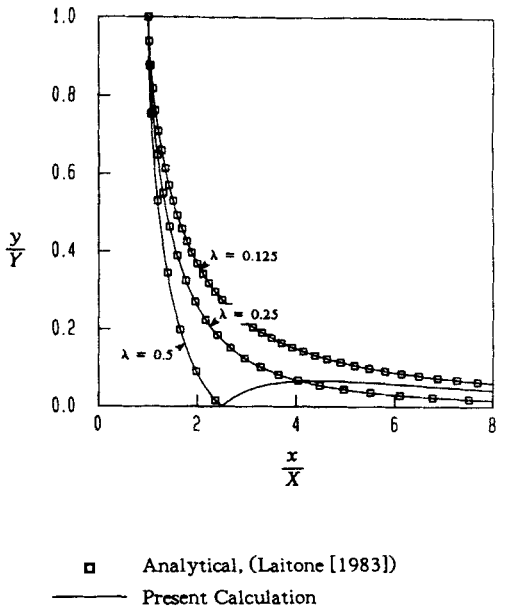

Figure 9. Comparison of calculated particle paths with the analytical solution from Laitone (1983) for stagnation point flow.

Turbulent flow past one and two in-lines tubes

Figure 10 shows the results predicted using the procedure described above, for the flow of air past two in-line tubes. The calculation conditions correspond to those of the particle flux experiments of Schweitzer and Humphrey (1988); $Re = 2.94 \times 10^4$, $(L_t/D) = 4.1$, and $(L_t/D) = 5.0$ with $(k/U_\infty^2) = 0.021$ and $(\epsilon\mu/U_{\infty}^2\rho) = 7.28 \times 10^{-5}$ at the inlet, $T = 300$ K, $P = 101.3$ kPa. A grid consisting of 117 × 28 nodes was used. More refined grids did not yield significantly different results. Particle trajectories were simulated using these flow field results for $\lambda = 0.1$, 0.5, 1.0, and 10.0 both neglecting and considering the effect of turbulent velocity fluctuations. These values of λ correspond to glass beads, $\rho_{pt} = 2500$ kg/m^3, of 4.09, 9.15, 12.9, and 40.9 μm in diameter. The results obtained neglecting the effect of the fluctuations are discussed

Figure 11 shows predicted trajectories for particles unaffected by turbulence for different values of λ, corresponding to the flow illustrated in Figure 10. Gravity acts to the right in the figures (in the direction of the flow). The particles were released at the entrance to the calculation domain (not shown in the figure) in increments of $0.1D$ above the bottom symmetry plane with velocities $u_{pt} = u_\infty$. The first particle was released at a slight distance from the symmetry plane so that it would move into the flow field. Fluid flow conditions were the same as discussed for Figure 10. The restitution coefficients were set to $e_n = e_t = 0.3$ in these and all subsequent calculations. These values of e_n and e_t

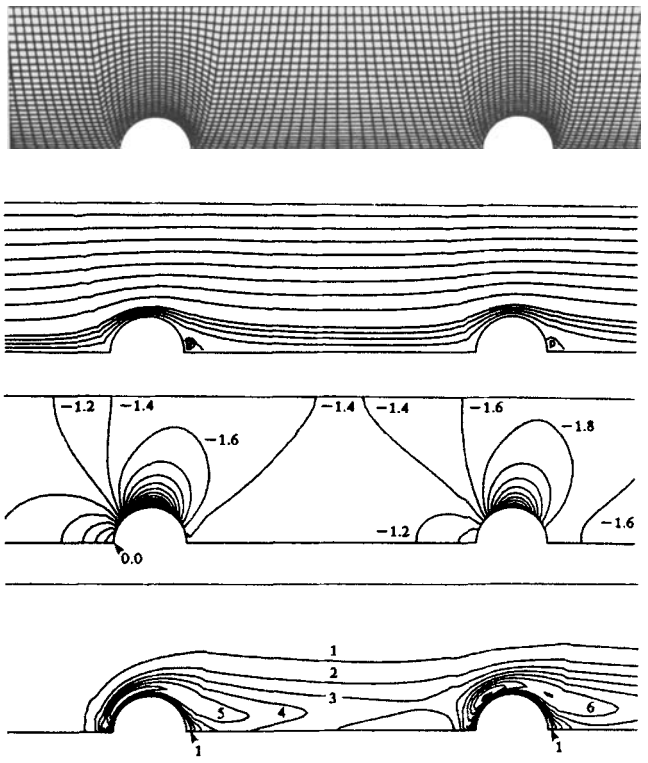

Figure 10. Flow field calculation using: a. 117 × 28 grid; b. streamlines; c. isobars; d. turbulent kinetic energy contours.

Streamline contour intervals are 0.025 and 0.1 for the bulk flow, and 0.001 for the recirculating flow. Isobar contour interval, $(P - P_{static}/(\frac{1}{2}\rho U_\infty^2)$, is 0.2. Turbulent kinetic energy contour interval, $100(k)/(U_\infty^2)$, is 1.0. The left- and righthand planes shown are at $(x/D) = 17.7$ and 26.6, respectively.

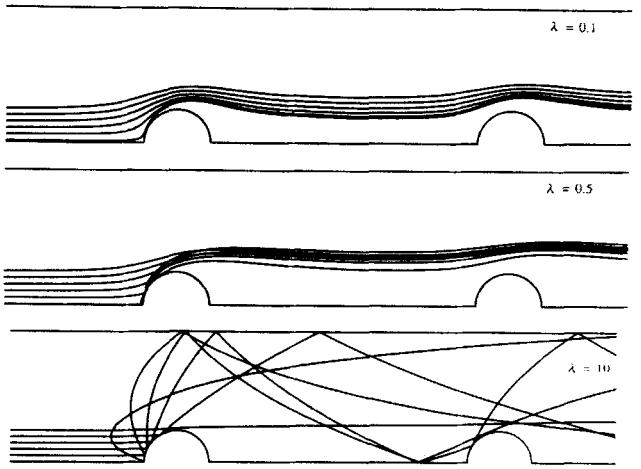

Figure 11. Particle paths for two in-line tubes showing the effect of the particle response time on collisions with the downstream tube.

Left- and righthand planes shown are at $(x/D) = 17.1$ and 26.7, respectively.

were determined by matching calculated rebound heights with corresponding photographic data in Schweitzer and Humphrey (1988). The results show that particles with $\lambda > 1$ are fairly inertial and experience substantial rebounding from a tube surface. The results for $\lambda = 10$ show that rebounding particles can cross the flow symmetry plane. Where this occurs, mirror-image particles are reintroduced in the flow, some of which will impact the second in-line tube.

Particle fluxes to the first of two in-line tube surfaces are shown in Figure 12 for $\lambda = 0.5$ and 10. They are compared to the theoretical maximum particle flux, which occurs when $\lambda = \infty$ for which all the particles released within $\frac{1}{2}$ D of the bottom symmetry plane strike the tube. Due to the curvature of the tube the resulting flux for this case has a cosine dependency on θ. The particle fluxes were calculated by releasing 100 particles at equally spaced intervals from the centerline to $\frac{1}{2}$ D above the

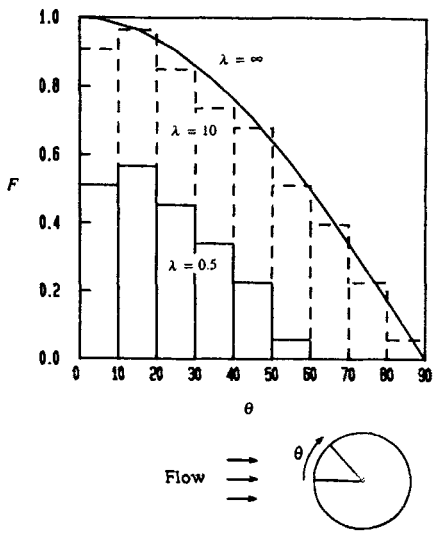

Figure 12. Particle fluxes to the surface of the first tube of two in-line tubes with $(L_t/D) = 5$.

Flow field conditions correspond to those of Figure 10.

bottom symmetry plane and counting the number of impacts occurring over 10° intervals on the tube surface. As expected, the particle flux decreases with decreasing λ since the particles become more responsive to the flow field in passage past the tubes.

A comparison of the particle fluxes to the first of two in-line tubes for two different fluid temperatures is shown in Figure 13a. The particles are 9.15 μm in diameter, which corresponds to $\lambda = 0.5$ at $T = 300$ K, and $\lambda = 0.22$ at $T = 1{,}000$ K, due to the dependence of μ on temperature. The velocity at the inlet plane is the same for both cases. At $T = 1{,}000$ K, the particle flux is larger for $\theta \leq 20°$ and smaller for $\theta > 20°$ compared with the 300 K case. This is explained by the stronger coupling through viscosity at 1,000 K. For $\theta \leq 20°$, particles deviating from the streamlines strike on the front of the tube. As they rebound with a decreased velocity, they interact with the flow field, which forces them to hit the tube again. This process is repeated several times until the particles finally escape, usually by sliding along the tube surface. On the other hand, for $\theta > 20°$ the particles follow the streamlines closely and do not strike the tube.

The particle speeds and impact angles at the instant of impact can be used to determine the relative wear on the tube surface by using Finnie's (1959, 1960) cutting wear model. This model was used by Dosanjh and Humphrey (1985) to predict the erosion of a plate by a particle-laden turbulent air jet. Given the impact information, the volume of material removed per unit time per unit area, Q, is given by

$$Q = \begin{cases} \dfrac{N_{pt} m_{pt} u_{pt}^2}{6\psi} \sin^2 \beta & 0.0° \leq \beta \; 71.5° \\ \dfrac{N_{pt} m_{pt} u_{pt}^2}{2\psi} [\sin(2\beta) - 3\cos^2 \beta] & 71.5° \leq \beta \leq 90° \end{cases} \tag{30}$$

where ψ is a wear model constant that depends on the material properties. The wear due to particle impact can be normalized by dividing Q by $(N_{pt} m_{pt} u_\infty^2 / 6\psi)$, so that the actual value of ψ is not required. In point of fact, ψ may depend weakly on T for the types of materials from which the tubes in a heat exchanger tube bank are likely to be made. For constant impact velocity, the model predicts maximum wear for impacts at $\beta = 73.2°$ relative to the surface normal.

Figure 13b shows the relative wear of the first of two in-line tubes due to particles in flow fields evaluated at $T = 300$ K and 1,000 K. These results show less erosion for the tube in the high temperature flow due to the stronger coupling, through viscosity, between the particle and the fluid motion. Both the extent and position of maximum wear are predicted to be strongly dependent on temperature.

Attention is now turned to the effect of the turbulent velocity fluctuations on particle motion. Figures 14 a, b and c show the calculations performed for three values of λ using the flow field results presented in Figure 10, this time considering the effects of the fluctuations on the particles. In each case, 20 particles were released at the entrance of the calculation domain (not shown in the figure), at a single location $\frac{1}{4} D$ above the bottom symmetry plane. These figures show that the importance of the fluctuations diminishes as λ increases, as predicted by the argument leading to Eq. 27. However, examination of Figure 14c reveals that even though a given fluctuation does not affect the motion of the particle significantly when $\lambda = 10$ (as indicated by

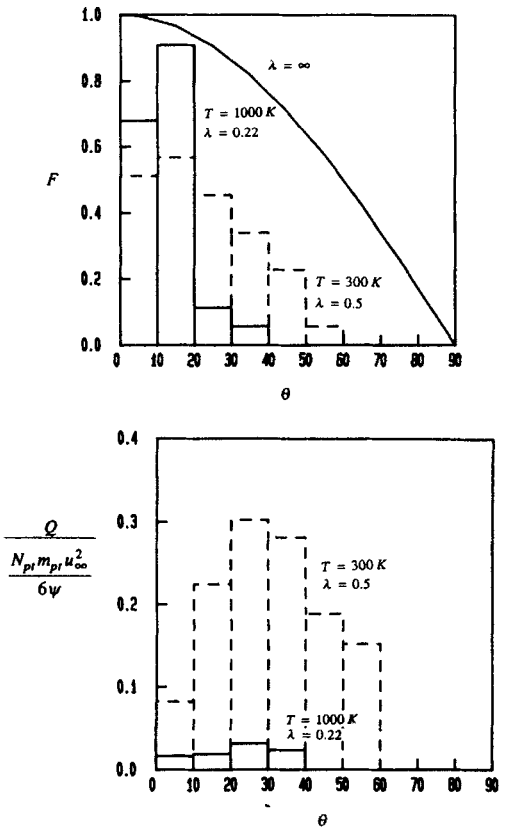

Figure 13. Temperature effects on the particle flux to the surface of the first of two in-line tubes and on its erosion, for the same particle size and inlet velocity: $d_{pt} = 9.15$ μm, $U_\infty = 19.2$ m/s.

a. Angular distribution of flux to the surface.
b. Angular dependence of surface erosion.

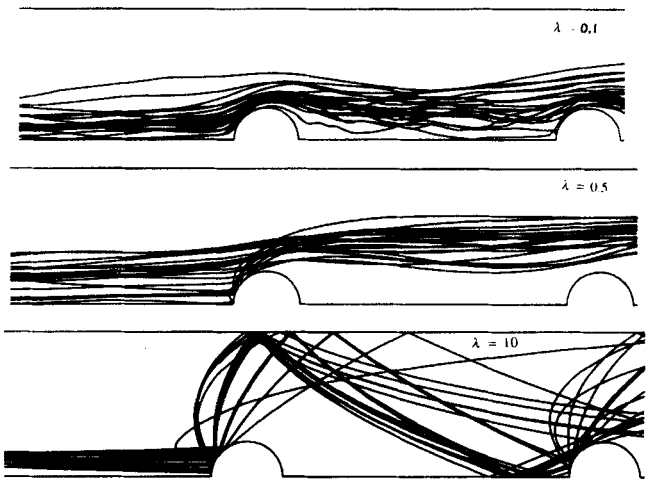

Figure 14. A comparison of particle paths for two in-line tubes showing the effect of different values of λ on the particle response to the turbulent fluctuations.

Fluid flow conditions correspond to those of Figure 10. Left- and righthand planes shown are at $(x/D) = 15.8$ and 25.4, respectively.

the relatively smooth trajectories), the random cumulative effects of the fluctuations result in different trajectories for different particles released at the same starting location. It is also interesting to note that, for $\lambda = 0.1$, some of the particles hit both the first and the second tube, a behavior not predicted when the effects of the fluctuations are ignored (see Figure 11). However, for $\lambda = 0.5$ and 10 the overall patterns of the deterministic and fluctuation trajectories is strikingly similar even though the individual particle trajectories differ.

Figure 15 shows a comparison between particle fluxes over the first of two in-line tubes for the conditions of Figure 10 with $\lambda = 0.5$ and 10. The theoretical maximum for particles with $\lambda = \infty$ is also shown. The effects of the turbulent fluctuations were considered by means of the SSF model with 40 particles being released at each of 100 equally spaced locations between the top and the bottom symmetry planes, for a total of 4,000 particles. Particle impacts were added over 10° increments on the tube surface and, as for the deterministic case, the flux to the tube is observed to decrease with decreasing λ.

The effect of temperature on the particle flux for two in-line tubes corresponding to the conditions of Figure 10 is shown in Figure 16a. Multiple reboundings are not present in this case since, following the first rebound, the fluctuating velocity field carries a particle away from the tube surface. The corresponding erosion comparison is shown in Figure 16b, where higher erosion rates are predicted for the fluctuating case than for the non-fluctuating. This is attributed to the higher particle velocities induced locally by the fluctuations.

Turbulent flow and particle paths in a tube bank

Figure 17a shows the streamlines for the flow past a tube in a rectangular tube bank with $Re = 25{,}600$ and $(L/D) = 2.0$. Particle trajectories for different λ are illustrated in Figures 17b, c and d. The trajectories have been calculated for nonfluctuating flow conditions for $\lambda = 0.1$, 1.0 and 10. (corresponding to particle diameters of 9.26, 29.3 and 92.6 μm, respectively). Three flow field cycles are computed for each λ. In the first cycle, the particles are released at $y = 1/4\ D$ with a velocity equal to the fluid velocity at that point. For each of the two subsequent cycles, the particles reenter the calculation domain at y locations

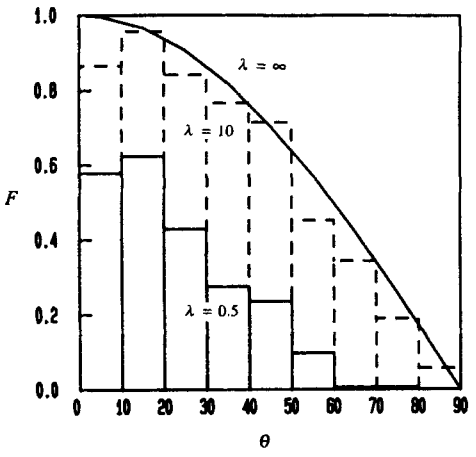

Figure 15. Particle fluxes to the surface of the first of two in-line tubes with $(L/D) = 5$.
Flow field conditions correspond to those of Figure 10.

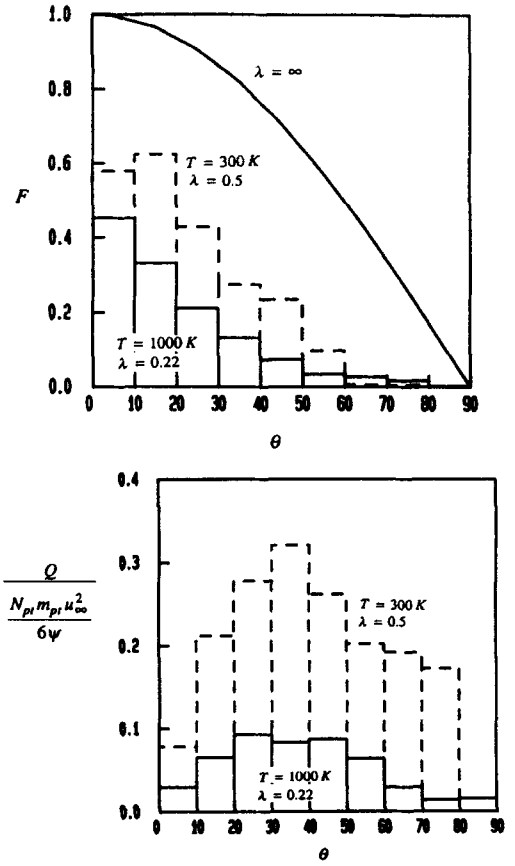

Figure 16. Temperature effects on the particle flux to the surface of the first of two in-line tubes and on its erosion, for the same particle size and inlet velocity: $d_{pi} = 9.15\ \mu$m, $U_\infty = 19.2$ m/s.

a. Angular distribution of flux to the surface.
b. Angular dependence of surface erosion.

corresponding to the previous y locations on the exit plane, and with the corresponding particle velocity at the exit plane. As expected, for low λ a particle is diverted and never hits the tube. However, with increasing λ the particle trajectories become complex due to tube reboundings that induce crossings of the symmetry planes.

Conclusions and Recommendations

A numerical procedure has been developed and tested that calculates 2*D*, steady, constant property flows in nonorthogonal body-fitted curvilinear coordinates. [The entire code is listed and documented in Schuh (1987) and is available on tape or IBM PC diskette from the authors at the University of California, at Berkeley.] It has been applied to predict laminar and turbulent flows past one and two in-line tubes, and past a tube in an infinite tube bank. For the turbulent flow cases, a two-equation $(k - \epsilon)$ model was used that relates the Reynolds stresses to the strain field via an isotropic turbulent viscosity. A logarithmic law-of-the-wall relation was used to connect the shear stress at the tube wall with the velocity in the turbulent part of the flow. Although prone to error in the vicinity of the separation point on the tube, the turbulence model has yielded results in good quali-

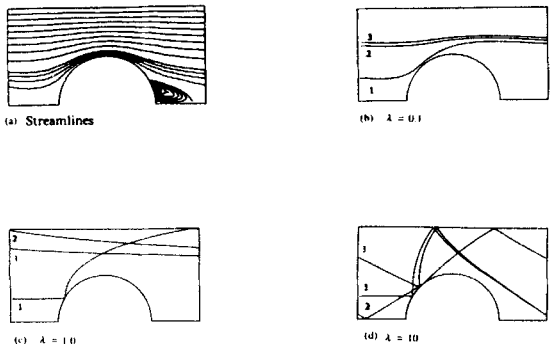

Figure 17. Flow field and particle paths for flow in a tube bank with $Re = 2.56 \times 10^4$ and $(L/D) = 2$.

a. Streamline contour intervals are 0.025 and 0.1 for the bulk flow and 0.001 for the recirculating flow.
b, c, d. Trajectory of a particle released between two tubes with: a. $\lambda = 0.1$; b. $\lambda = 1.0$; and c. $\lambda = 10.0$

tative agreement with the test cases examined. Testing in the laminar flow regime has yielded results in excellent quantitative agreement with the measurements and calculations of others.

The assumption of one-way coupling has allowed the prediction of particle speeds and trajectories for dilute noninteracting particle-laden gas flows for some of the tube configurations examined. For this, a deterministic particle equation of motion formulated in Lagrangian coordinates was used. The calculations yield the necessary impact velocity information from which to evaluate particle flux to, and erosion of, tube surfaces. The predictions show that particles in flows with $\lambda < 1$ follow the streamlines fairly closely, while those with $\lambda > 1$ do not. As a result, the latter induce higher rates of wear than the former and are more likely to rebound from several consecutive tubes in a tube bank. Because the value of λ decreases with increasing gas viscosity, particles in flow fields at high temperatures are expected to follow the streamlines more closely and, as a result, erode less.

The effect of the turbulent velocity fluctuations was explored using a simplified SSF model. Calculations show that the effect of the fluctuations is very important for $\lambda < 1$, since these particles are very responsive to changes in the flow field. Over long times, the history of the fluctuations can also affect the trajectories of inertial particles ($\lambda > 1$).

For fixed Reynolds number, the characteristics of the computed fluid flow fields show a strong dependence on the spacing between tubes, especially in the mean flow direction. Thus, in closely spaced tube configurations the front of a tube is shielded from direct particle impacts by the tube ahead of it. The optimum tube spacing in a tube bank represents a compromise among the wear, pressure drop and heat transfer requirements of the bank. The present numerical procedure provides a valuable design tool for investigating arbitrary tube configurations and flow conditions of practical interest.

Acknowledgements

This research was sponsored by Martin Mariette Energy Systems, Inc. (Subcontract #19X-55936C) under their Principal Contract with the U.S. Department of Energy # DE-AC05-84OR21400. Additional support was received by the second author in the form of a scholarship from MARAVEN S.A., subsidiary of Petroleos de Venezuela S.A. Both sources of support are gratefully acknowledged.

Notation

A = convection-diffusion coefficient, Eq. 15; also used as area
A_{pt} = projected area of the particle
$\boldsymbol{a}^i$ = contravariant base vectors
$\boldsymbol{a}_i$ = covariant base vectors
b = source term in general convection-diffusion equation, Eq. 14
C_D = constant for the dissipation term in the turbulent kinetic energy equation, Eqs. 7 and 13
C_{Dr} = drag coefficient for the particle, Eq. 18
C_P = local cell mass imbalance
C_1 = constant for the generation term in the dissipation of turbulent kinetic energy equation, Eqs. 8 and 13
C_2 = constant for the dissipation term in the dissipation of turbulent kinetic energy equation, Eqs. 8 and 13
C_μ = constant for the turbulent viscosity equation, Eqs. 12 and 13
D = diameter of a tube
d_{pt} = particle diameter
e_n = normal restitution coefficient
e_t = tangential restitution coefficient
F = nondimensional particle Flux over the tube surface, $F = (N_{pt}/N_o\Delta\theta)$
f = correction factor for the Drag Coefficient, Eq. 19
G = generation of turbulent kinetic energy, Eq. 9
g = square of the Jacobian
g^{ij} = component of the contravariant metric tensor
g_{ij} = component of the covariant metric tensor
$\boldsymbol{g}$ = acceleration due to gravity
$\sqrt{g}$ = Jacobian
i = index—$i = 1$, 2, and 3 for three dimensions and $i = 1$ and 2 for two dimensions
$\hat{\imath}$ = unit base vector for the cartesian coordinate system
j = index—$j = 1$, 2, and 3 for three dimensions and $j = 1$ and 2 for two dimensions
$\hat{\jmath}$ = unit base vector for the cartesian coordinate system
k = turbulent kinetic energy
L = distance between the centers of two tubes in a rectangular infinite tube bank with equal longitudinal and transverse spacing
L_l = longitudinal distance between the centers of two tubes in a rectangular infinite tube bank
L_t = transverse distance between the centers of two tubes in a rectangular infinite tube bank
L_{ref} = characteristic length of the flow field
L_ϵ = integral dissipation scale
m = erosion proportional to the fluid velocity to the power m
m_{pt} = mass of the particle
N_{pt} = number of particles that hit the tube in a given angle interval of the tube surface
N_o = number of particles released at the entrance of the calculation domain between the bottom symmetry plane and $\frac{1}{2}D$
P = pressure
P = source term in the elliptic grid generation equation that controls the verticle lines
Q = volume of material removed per unit time per unit area by N particles each of mass m_{pt}, Eq. 30
Q = source term in the elliptic grid generation equation that controls the horizontal lines
Re = Reynolds number, $(\rho u_\infty D/\mu)$
Re_{pt} = particle Reynolds number, $(\rho|U - U_{pt}|d_{pt}/\mu)$
$\boldsymbol{r}$ = vector location of a point, $\boldsymbol{r} = x\hat{\imath} + y\hat{\jmath}$
t = time
t_{EDDY} = lifetime of a turbulent eddy
S_u = source term for the convection-diffusion, Eq. 15
S_P = source term for the point of interest in the convection-diffusion equation
U^i = contravariant velocity component
U_{ref} = reference velocity
$\boldsymbol{U}$ = vector velocity of the fluid
$\boldsymbol{U}_{pt}$ = vector velocity of the particle
u = x component of the fluid vector velocity
u' = velocity scale of the turbulent fluctuations
u_∞ = free stream velocity for single tubes and two tubes *in tandem;* average velocity at the minimum cross section, $\bar{u}_{mcs}$ for infinite tube banks
u_{pt} = x component of the particle vector velocity

u'_{pt} = x component of the particle vector velocity after rebound
v = y component of the fluid vector velocity
v_{pt} = y component of the particle vector velocity
v'_{pt} = y component of the particle vector velocity after rebound
w_n = particle velocity component normal to the boundary
w'_n = particle velocity component normal to the boundary after rebounding
w_t = particle velocity component tangential to the boundary
w'_t = particle velocity component tangential to the boundary after rebounding
x = Cartesian coordinate location
y = Cartesian coordinate location

Greek letters

β = particle impact angle relative to surface normal
Γ = general diffusion constant, Eq. 14
$\Delta\theta$ = angle interval on the boundary surface
δ = small distance or number
ϵ = dissipation of turbulent kinetic energy
ζ = another name for ξ^1
η = another name for ξ^2
θ = angle on the boundary surface, Figure 5
κ = Von Karman constant
λ = nondimensional particle response time, or momentum equilibrium constant, Eq. 21
μ = dynamic viscosity
μ_e = effective dynamic viscosity, Eq. 11
μ_t = turbulent viscosity, Eq. 12
ξ^i = ith curvilinear coordinate
ρ = density of the fluid
ρ_{pt} = density of the particle
σ_k = constant in turbulent kinetic energy equation, Eqs. 7 and 13
σ_ϵ = constant in the dissipation of turbulent kinetic energy equation, Eqs. 8 and 13
τ = particle response time, $\tau = (\rho_{pt} d_{pt}^2/18\mu)$
ϕ = arbitrary variable, u, v, P, k, and ϵ, Eq. 14
ψ = wear model constant, Eq. 30

Subscripts

E = value at the point to the east of the control volume
N = value at the point to the north of the control volume
pt = particle
S = value at the point to the south of the control volume
W = value at the point to the west of the control volume

Literature Cited

Achenbach, E., "On the Cross Flow through In-Line Tube Banks with Regard to the Effect of Surface Roughness," *Wärme und Stoffübertragung*, **4**, 152 (1971).

Acrivos, A., L. G. Leal, D. D. Snowden, and F. Pan, "Further Experiments on Steady Separated Flows Past Bluff Objects," *J. Fluid Mech.*, **34**(1), 1, 25 (1968).

Antonopoulos, K. A. "Prediction of Flow and Heat Transfer in Rod Bundles," Ph.D. Thesis, Imperial College of Science and Technology, London (1979).

———, "Heat Transfer in Tube Banks Under Conditions of Turbulent Inclined Flow," *Int. J. Heat and Mass Transf.*, **28**(9), 1645 (1985).

Benchaita, M. T., P. Griffith, and E. Rabinowicz, "Erosion of Metallic Plate by Solid Particles Entrained in a Liquid Jet," *J. of Eng. for Ind.*, **105**, 215 (1983).

Bergelin, O. P., G. A. Brown, and S. C. Doberstein, "Heat Transfer and Fluid Friction During Viscous Flow Across Banks of Tubes—IV, A Study of the Transition Zone Between Viscous and Turbulent Flow," *Trans. ASME*, **74**, 953 (1952).

Boothroyd, R. G., *Flowing Gas-Solids Suspensions*, Chapman and Hall, London (1971).

Celik, I., V. C. Patel, and L. Landweber, "Calculation of the Mean Flow Past Circular Cylinders by Viscous-Inviscid Interaction," *J. of Fluids Eng.*, **107**, 218 (1985).

Chilukiru, R., and D. A. Steininger, "Large Eddy Simulation of Turbulent Buffeting Forces in Steam Generator Tube Banks," BHRA Int. Conf. on Flow Induced Vibrations, England (1987a).

———, "Numerical Simulation of Turbulence Deep within Heat Exchanger Tube Bundles," ASME PVP Conf., San Diego, CA (1987b).

Clift, R., J. R. Grace, and M. E. Weber, *Bubbles, Drops, and Particles*, Academic Press, New York (1978).

Coutanceau, M., and R. Bouard, "Experimental Determination of the Main Features of the Viscous Flow in the Wake of a Circular Cylinder in Uniform Translation: 1. Steady flow," *J. Fluid Mech.*, **79**(2), 231 (1977).

Dosanjh, S., and J. A. C. Humphrey, "The Influence of Turbulence on Erosion by a Particle-Laden Fluid Jet," *Wear*, **102**, 309 (1985).

Faghri, M., and N. Rao, "Numerical Computation of Flow and Heat Transfer in Finned and Unfinned Tube Banks," *Int. J. Heat and Mass Transf.*, **30**(2), 363 (1987).

Finnie, I., "An Experimental Study of Erosion," *Proc. Soc. Exp. Stress Analy.*, **17**(2), 65 (1959).

———, "Erosion of Surfaces by Solid Particles," *Wear*, **3**, 87 (1960).

Fujii, M., T. Fujii, and T. Nagata, "A Numerical Analysis of Laminar Flow and Heat Transfer of Air in an In-Line Tube Bank," *Num. Heat Transf.*, **7**, 89 (1984).

Grove, A. S., F. H. Shair, E. E. Petersen, and A. Acrivos, "An Experimental Investigation of the Steady Separated Flow Past a Circular Cylinder," *J. of Fluid Mech.*, **19**, 60 (1964).

Laitone, J. A., "Aerodynamic Effects in the Erosion Process," *Wear*, **56**, 239 (1979a).

———, "Erosion Prediction Near a Stagnation Point Resulting From Aerodynamically Entrained Solid Particles," *J. Aircraft*, **16**(12), 809 (1979b).

———, "Separation Effects in Gas-Particle Flows at High Reynolds Numbers," LBL-9996, Ph.D. Thesis (1979c).

———, "Characterization of Particle Rebound Phenomena in the Erosion of Turbomachinery," *J. Aircraft*, **20**(3), 275 (1983).

Laufer, J., "Investigation of Turbulent Flow in a Two-Dimensional Channel," Technical Note 2123, National Advisory Committee for Aeronautics (1950).

Launder, B. E., and T. H. Massey, "The Numerical Prediction of Viscous Flow and Heat Transfer in Tube Banks," *J. of Heat Transf.*, **100**, 565 (1978).

Launder, B. E., and D. B. Spalding, "The Numerical Computation of Turbulent Flows," *Comp. Methods in Appl. Mech. and Eng.*, **3**, 269 (1974).

Majumdar, S., and W. Rodi, "Numerical Calculations of Turbulent Flow Past Circular Cylinders," Symp. on Numerical and Physical Aspects of Aerodynamic Flows, Long Beach, CA (1985).

Ormancey, A., and J. Martinon, "Prediction of Particle Dispersion in Turbulent Flows," *Physico-Chem. Hyrdody.*, **1**(3/4), 229 (1984).

Patankar, S. V., C. H. Liu, and E. M. Sparrow, "Fully Developed Flow and Heat Transfer in Ducts Having Streamwise-Periodic Variations of Cross-Sectional Area," *J. of Heat Transf.*, **99**, 180 (1977).

Patankar, S. V., *Numerical Heat Transfer and Fluid Flow*, Hemisphere Publishing (1980).

Pourahmadi, F., and J. A. C. Humphrey, "Modeling Solid-Fluid Turbulent Flows with Application to Predicting Erosive Wear," *Physico-Chem. Hydrody.*, **4**(3), 191 (1983).

Press, W. H., B. P. Flannery, S. A. Teukolsky, and W. T. Vetterling, *Numerical Recipes*, Cambridge Univ. Press (1986).

Rodi, W., "Examples of Turbulence Model for Incompressible Flows," *AIAA J.*, **20**(7), 872 (1982).

———, *Turbulence Models and Their Application in Hydraulics—A State of the Art Review*, 2nd ed., Int. Assoc. for Hydraulic Research, Delft, Netherlands (1984).

Schuh, M. J., "Numerical Prediction of Fluid and Particle Motions in Flows Past Tubes," Ph.D. Thesis, Univ. of California, Berkeley (1987).

Schweitzer, M. O., and J. A. C. Humphrey, "Note on the Experimental Measurement of Particle Flux to One and Two In-Line Tubes," *Wear*, **126**, 211 (1988).

Shuen, J-S., Chen, L-D., and G. M. Faeth, "Predictions of the Structure of Turbulent, Particle-Laden Round Jets," *Proc. AIAA Aerospace Sci. Meeting*, Reno, NV (1983).

Shuen, J-S., A. S. P. Solomon, Q-F. Zhang, and G. M. Faeth, "Structure of Particle Laden Jets: Measurements and Predictions," *AIAA J.*, **23**(3), 396 (1985).

Taneda, S., "Experimental Investigation of the Wakes behind Cylinders

and Plates at Low Reynolds Numbers," *J. Phys. Soc. of Japan*, **11**(3), 302 (1956).
Thompson, J. F., "A Survey of Dynamically-Adaptive Grids in the Numerical Solution of Partial Differential Equations," *Appl. Num. Math.*, **1**, 3 (1985).
———, "Numerical Grid Generation," A Short Course, Mississippi State Univ. June 9–13 (1986).
———, "A Composite Grid Generation Code For General 3-D Regions," AIAA-87-0275, *AIAA Aerospace Sciences Meeting*, Reno, NV (1987).
Thompson, J. F., Z. A. Warsi, and C. W. Mastin, *Numerical Grid Generation, Foundations and Applications*, North-Holland, New York (1985).
Vittal, B. V. R., and W. Tabakoff, "Effect of Solid Particles in Two Phase Flow Around A Two Dimensional Cylinder," AIAA-86-0349, *AIAA Aerospace Sciences Meeting*, Reno, NV (1986).
Zukauskas, A., "Heat Transfer from Tubes in Crossflow," *Adv. in Heat Trans.*, **8**, 93 (1972).
Zukauskas, A., and J. Ziugzda, *Heat Transfer of a Cylinder in Crossflow*, Hemisphere Publishing (1985).

Manuscript received Mar. 29, 1988 and revision received Nov. 1, 1988.